Supporting Information

Dangendorf et al. 10.1073/pnas.1616007114

SI Text

For comparing our GMSL curve with historical runs from CMIP5 models, we have used the sum of individually modeled contributions obtained by ref. 12. In this model data set, the output of the historical runs from CMIP5 climate models were used to derive GMSL contributions for the period 1900–2005. These contributions include: GMSL changes resulting from thermal expansion, corrected for drifts with the respective pre-industrial control runs; glacier contributions obtained by forcing a global glacier evolution model with CMIP5 air temperatures and precipitation; and surface mass balance estimates from Greenland and Antarctica ice sheets. Contributions from TWS for the period 1900–2005 and from observed ice sheet dynamic processes (only for the period 1993–2005, as it is assumed to be negligible before) were also included. Further details on the computation can be found in ref. 12.

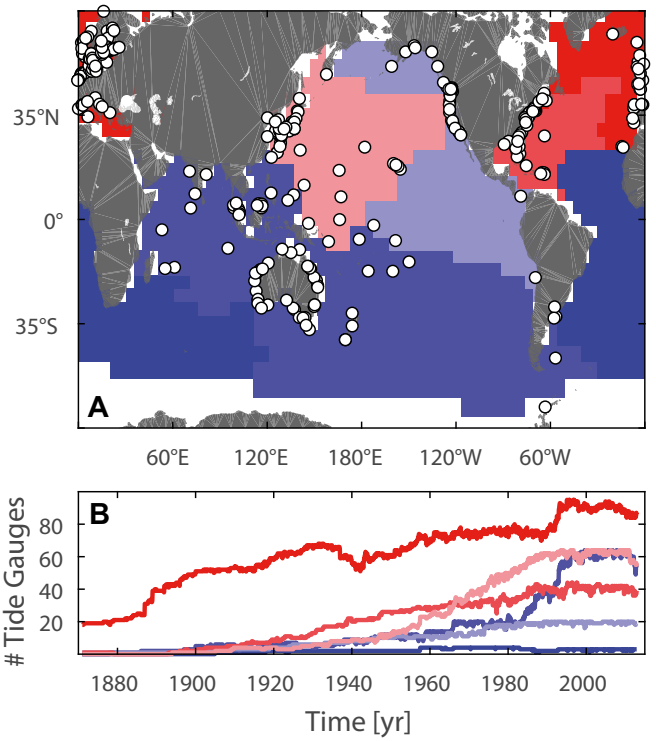

Fig. S1. Spatial and temporal availability of tide gauges used in this study. (*A*) Spatial distribution of the tide gauges used in this study. Also shown are the six oceanic regions, which are used to build regional virtual stations. (*B*) Respective temporal availability of tide gauges for each region.

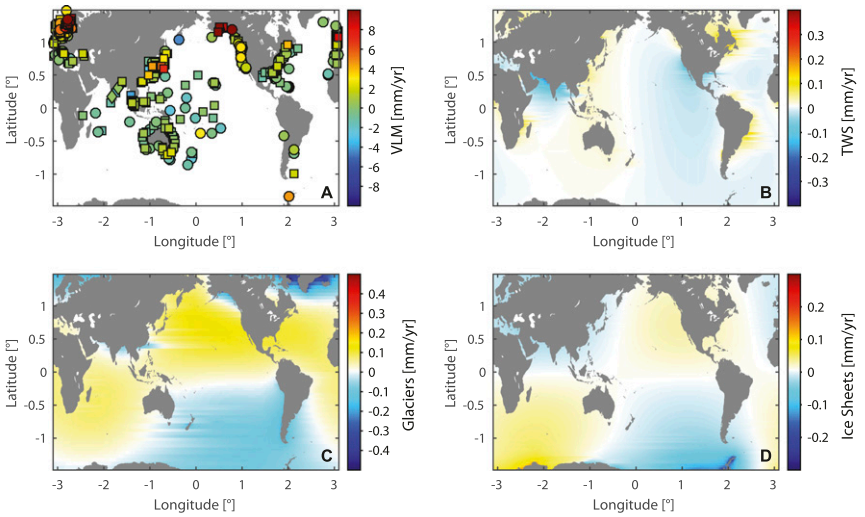

Fig. S2. Solid Earth and geoid corrections used in this study. (*A*) VLM [circles, GPS; square, altimetry minus tide gauge (AL-TG); diamonds, GIA] and geoid corrections resulting from (*B*) TWS, (*C*) glaciers, and (*D*) ice sheets.

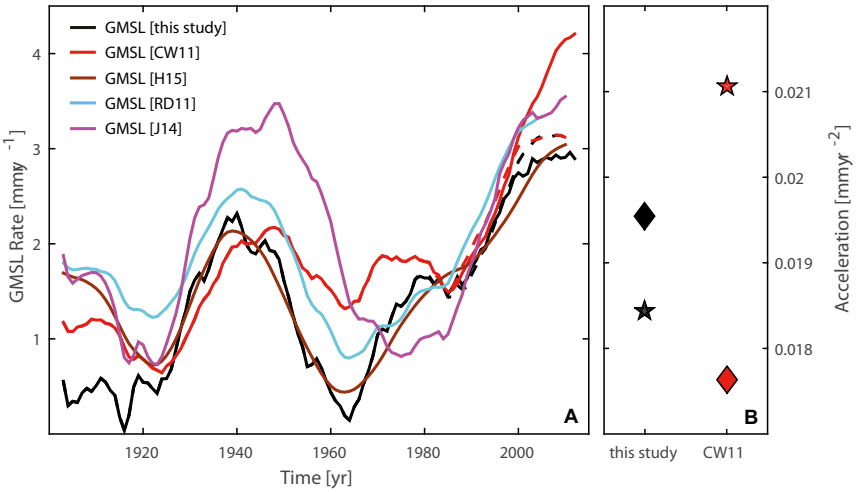

Fig. S3. Comparison of GMSL rates from tide gauges and satellite altimetry. (*A*) Shown are the GMSL rates from ref. 1 (red) and our reconstruction (black), once based solely on tide gauges (solid lines), and once adjusted for GMSL from satellite altimetry (AVISO) since 1993 (dotted line). For comparison, the rates from ref. 2 (cyan), ref. 5 (magenta), and ref. 6 (brown) also are shown. (*B*) The corresponding acceleration coefficients (diamonds, adjusted; pentagrams, original). The figure demonstrates that the ref. 1 reconstruction overestimates GMSL since 1993 by up to 1 mm·y^{-1}, leading to a very large acceleration over the entire century. However, once adjusted for the "true" GMSL from AVISO satellite altimetry since 1993, the adjusted reconstructions closely follow our original reconstruction, leading to an overall acceleration that is smaller than that estimated for our original GMSL reconstruction.

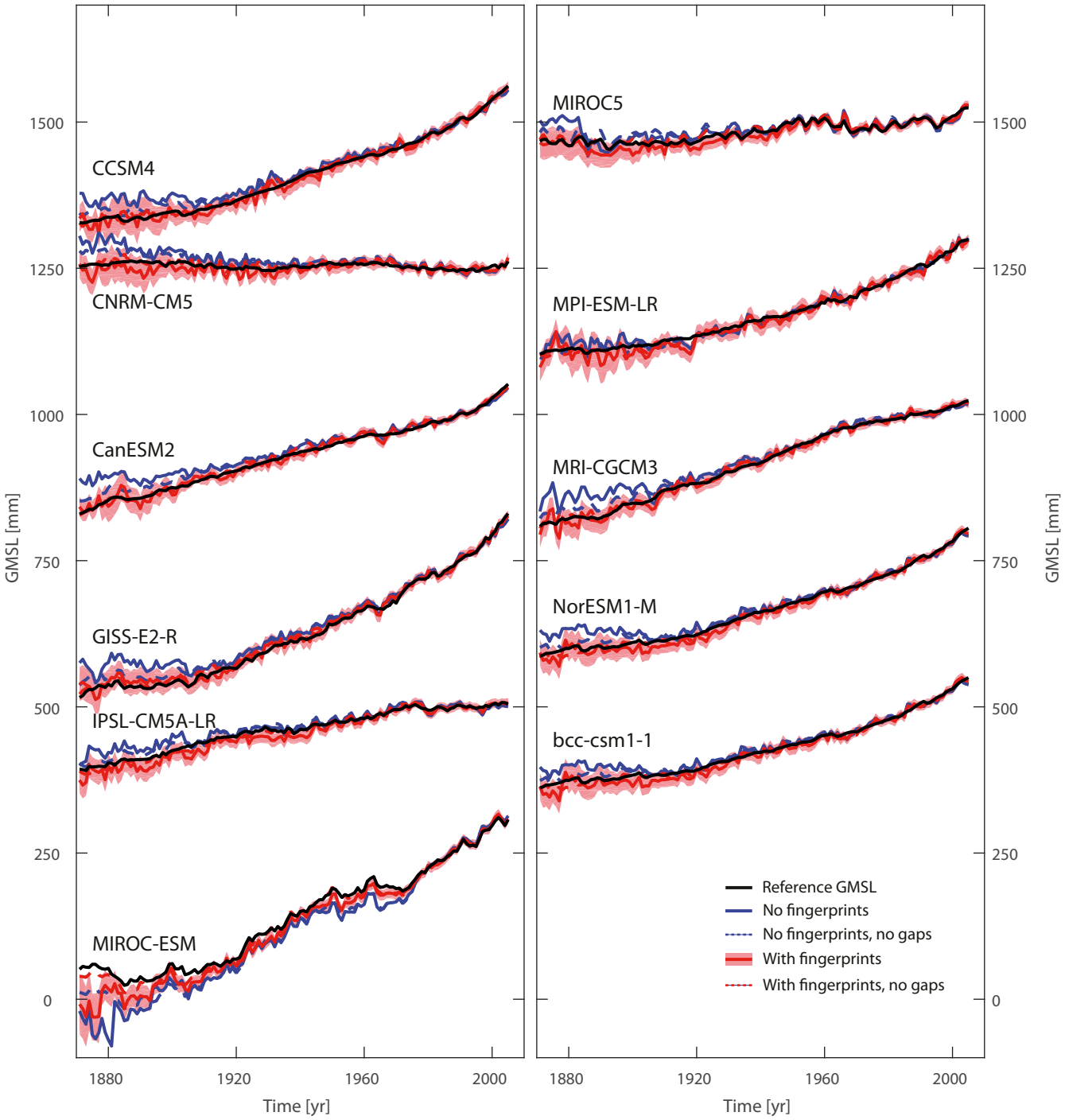

Fig. S4. Performance of the area-weighted average technique in synthetic sea level fields from the CMIP5 database. Comparison of reconstructed GMSL with the "true" reference GMSL in the 11 synthetic sea level fields based on CMIP5 historical simulations (dynamic sea level and glaciers) and reanalysis estimates of TWS and ice sheet melting. The sensitivity is tested for different initial data sets, as defined in the caption of Fig. 2 (showing the results for the GMSL from the SODA reanalysis).

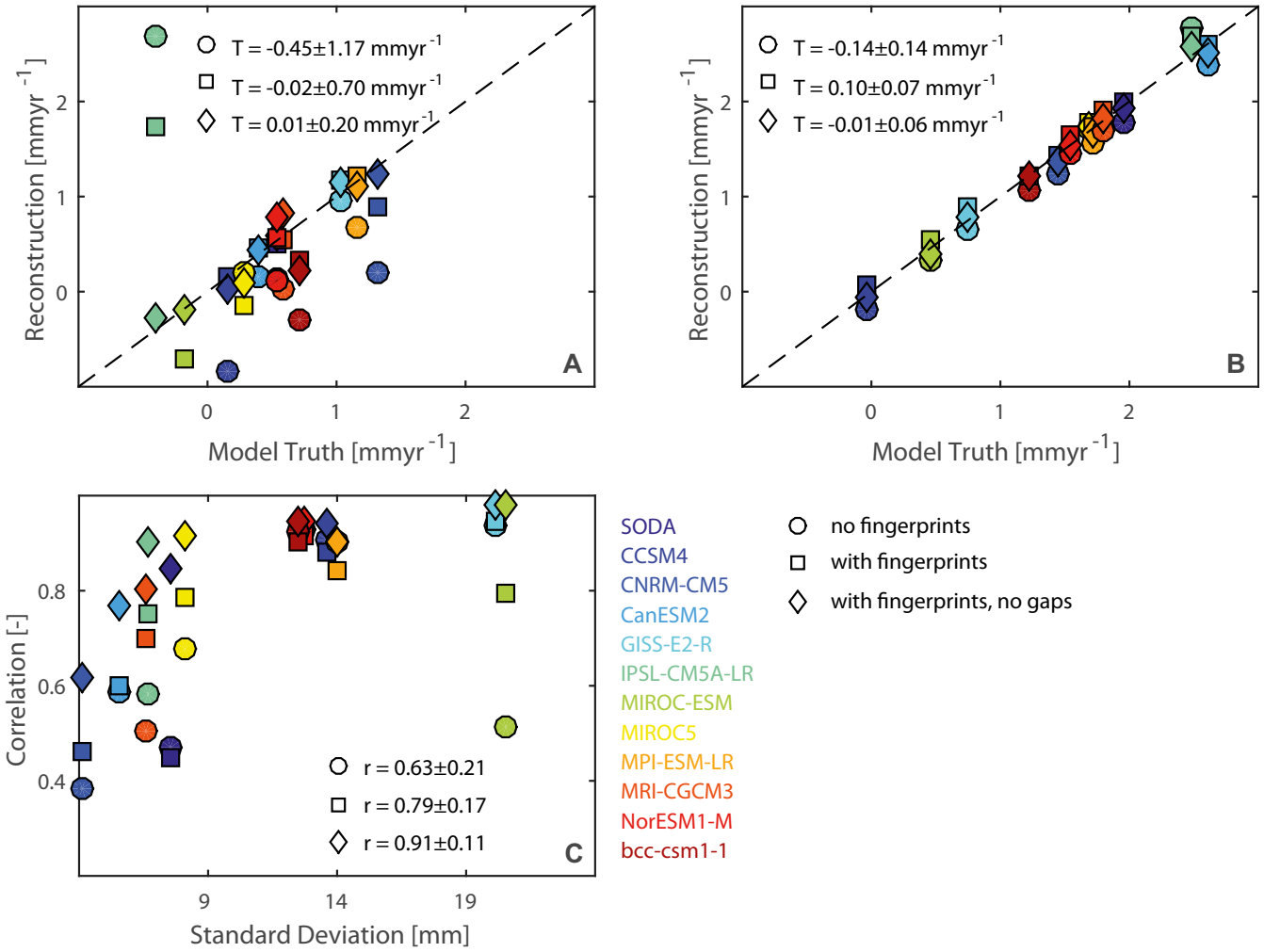

Fig. S5. Trend and correlation biases in GMSL reconstructions based on synthetic sea level fields from ocean models. (*A*) Comparison between the linear trends for the reference GMSL of each model and its reconstruction based on tide gauges with (squares) and without (circles) fingerprint corrections and assuming no gaps in tide gauge records (i.e., a fully available record; diamonds) for the period 1871–1902. (*B*) As *A*, but for the period 1902–2005. (*C*) Relationship between the correlation of the reference GMSL and its tide gauge reconstruction in each model and the respective interannual variability of the reference GMSL (SD). The results suggest that the GMSL can be better reconstructed in models with stronger interannual variability.

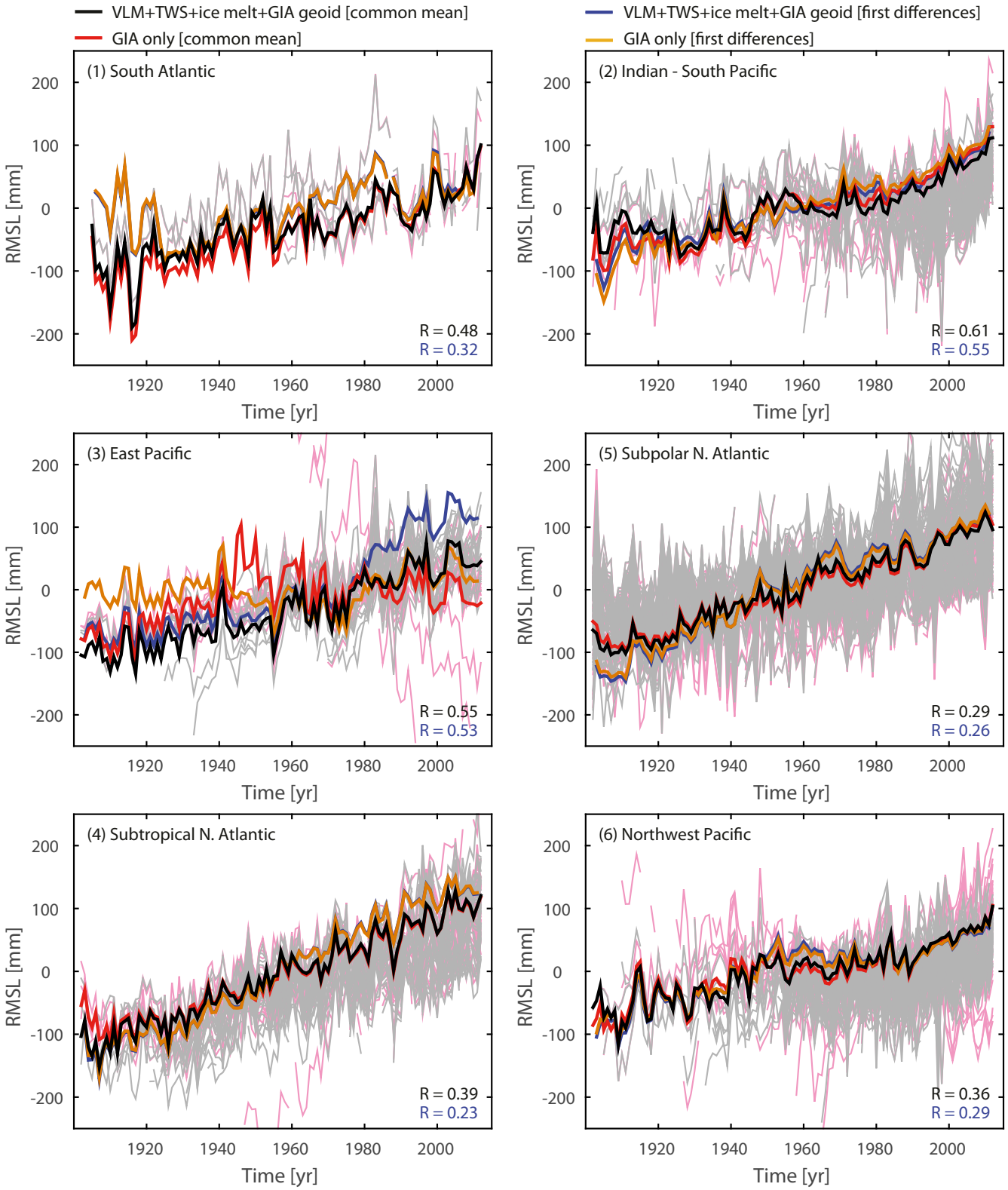

Fig. S6. Virtual stations for the six oceanic regions based on different stacking approaches and corrections. Shown are the individual tide gauge records corrected for VLM, TWS, ice melting, and GIA geoid (gray) or just GIA (light red) and their respective virtual stations based on two different stacking approaches: averaging after removing a common mean, and stacking first differences (also known as rate stacking; see legend for a description of the line colors). Both approaches are used to overcome the problem of an unknown reference datum of individual tide gauges. Also provided for each region are the medians of linear correlations between the virtual stations and individual tide gauge records from both approaches (black and blue R values).

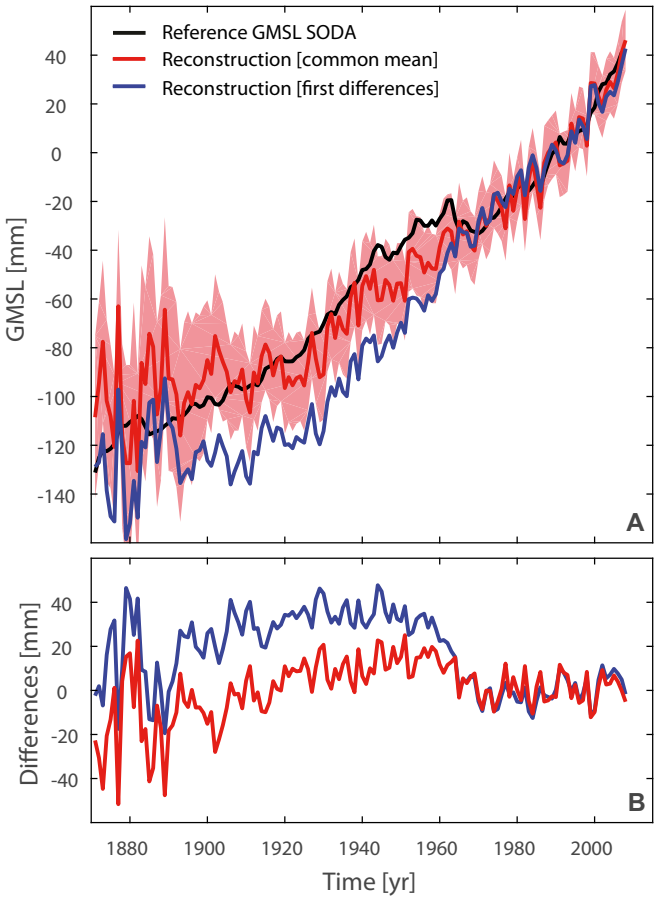

Fig. S7. Comparison of the reference GMSL in SODA to two different reconstructions. (*A*) Reference GMSL (black line) and reconstructions using either a common mean between individual tide gauges (red line, shaded area gives the 1σ uncertainty) or first differences (blue curve). (*B*) Differences between the reference GMSL and the two reconstructions.

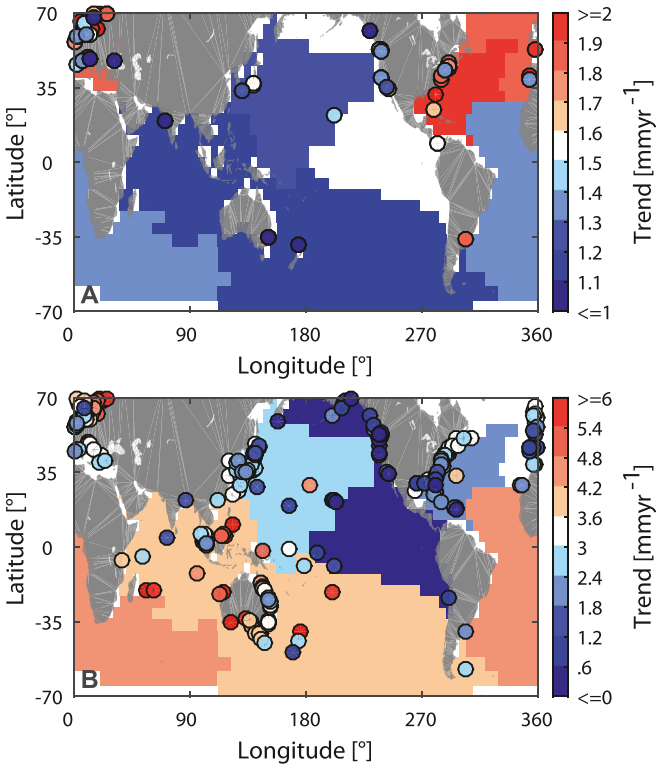

Fig. S8. Trends in individual tide gauges corrected for VLM and geoid changes from TWS and ice melt. (*A*) Trends in tide gauges providing at least 70 y of data during the period 1902–2012. Blue colors denote trends equal or smaller than 1.5 mm·y^{-1}, and white and red dots mark those stations providing long-term trends above 1.5 mm·y^{-1}. The colored shaded areas represent the trends of the region-specific virtual stations. (*B*) Trends in tide gauge records providing at least 15 y of data during the period 1993–2012. Blue colors denote trends equal or smaller than 3 mm·y^{-1}, whereas white and red dots mark those stations providing long-term trends above 3 mm·y^{-1}.

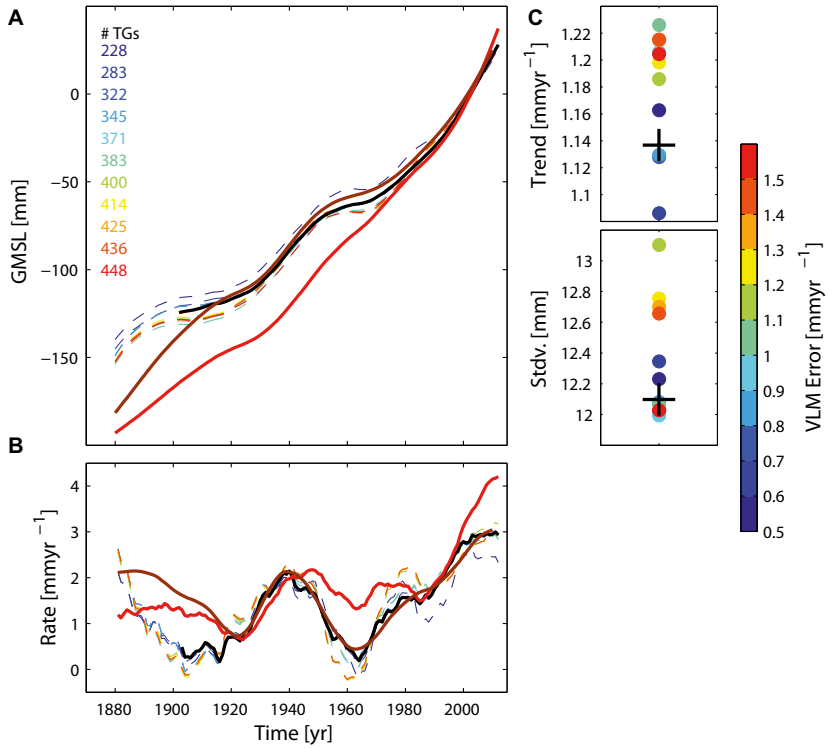

Fig. S9. Effect of tide gauge selection on GMSL and extension to 1880. (*A*) Shown are 11 realizations of our GMSL curve, using different subsets of tide gauges resulting from VLM error thresholds between 0.5 and 1.5 mm·y^{-1}, extending back to 1880 (dashed lines). Since before 1902, there is no information on the geoid corrections; these curves are corrected only for VLM. The GMSL curve from Fig. 3*A*, including all corrections, is shown for comparison in black. Also shown are the reconstructions from refs. 1 and 6 (solid red and brown lines, respectively). (*B*) Corresponding rates. (*C*) Linear trends (1902–1990) and SDs (1902–2012) from each reconstruction (colored dots) shown in *A* and the final curve from Fig. 3*A* (black cross).